Polyhedron 102 (2015) 615–626

Contents lists available at ScienceDirect

Polyhedron

journal homepage: www.elsevier.com/locate/poly

Synthesis, characterisation, electrochemical study and photovoltaic measurements of a new terpyridine and pyridine-quinoline based mixed chelate ruthenium dye

Binitendra Naath Mongal [a], Arunava Pal [b], Tarun Kanti Mandal [c], Jayati Datta [b,*], Subhendu Naskar [a,*]

[a] Department of Chemistry, Birla Institute of Technology, Mesra, Ranchi 835215, Jharkhand, India
[b] Electro-chemistry and Non-Conventional Energy Laboratory, Indian Institute of Engineering Science and Technology, Shibpur, Howrah 711103, West Bengal, India
[c] Department of Biotechnology, Haldia Institute of Technology, Hatiberia, Haldia 721 657, West Bengal, India

ARTICLE INFO

Article history:
Received 29 June 2015
Accepted 16 October 2015
Available online 29 November 2015

Keywords:
Ruthenium photosensitiser
MLCT
Pourbaix diagram
Ru-aquo species
DFT

ABSTRACT

A novel ruthenium-terpyridine based photosensitizer, Ru[(*p*-F-tpy)(pcqH)Cl] PF_6 (**1**); (*p*-F-tpy = 4′-(4-fluorophenyl)-2,2′:6′,2″-terpyridine, pcqH = 2-(2-pyridyl)-4-carboxyquinoline) was synthesized and spectroscopically characterized. The electronic spectrum of the complex shows the lowest energy MLCT band at 536 nm in DMSO. The ground state pK_a values of the acidic ligand (pcqH) and the Ru complex were spectrophotometrically determined. The pK_a of the COOH group in the free ligand is 3.56, and this reduces to 2.89 when bound to the metal. The cyclic voltammetry of the complex shows a reversible $Ru^{II/III}$ oxidation at 0.825 V with respect to Ag/AgCl reference electrodes in DMF. The Cl group is very labile, substitution of the Cl group by H_2O generates aqua species, which has been shown spectrophotometrically. A Pourbaix diagram for the Ru-aqua species has been constructed to show the detailed redox properties of the complex by means of cyclic voltammetry and differential pulse voltammetry at variable pH. Non-linear regression analysis was performed to generate the pK_a values for the Ru-aqua species as 11.89 (Ru^{II}) and 4.00 (Ru^{III}). Photovoltaic measurements with the dye were performed after anchoring onto a TiO_2 surface with the I^-/I_3^- redox electrolyte. Photovoltaic properties, like open-circuit photo-voltage (Voc = −0.35 V), short-circuit photocurrent density (J_{sc} = 1.428 × 10^{-4} amp cm^{-2}), fill factor (ff = 39.4%) and solar-to-electric conversion efficiencies (η = 0.13%), of the DSSCs constructed from the [Ru(*p*-F-tpy)(pcqH)Cl] PF_6 sensitized TiO_2 electrodes were measured. A DFT and TDDFT study has been performed on the complex. The TDDFT calculated absorption spectrum nicely matches the experimental spectrum.

1. Introduction

Photosynthesis has inspired the scientific community to design molecular systems to effectively trap sunlight as a source of alternative energy. Polypyridyl complexes of transition metals with a d^6 electronic configuration have the capability of absorbing light. Therefore these complexes can act as effective photosensitisers, just like chlorophyll-*b* or *b*-carotenoid in PSII [1–3]. With this goal, extensive research has been carried out on Ru-bipyridyl, phenanthroline and other related diimine complexes [4–18]. Ru(bipyridine)$_3^{+2}$ has evolved as the most effective photosensitiser over the years due to its photophysical novelty (an excited state lifetime of 1100 ns) [19], structural robustness and close proximity of the $Ru^{II/III}$ oxidation to that of the Photosystem-II [1,2]. However for the Ru(bpy)$_3^{+2}$ system with substituted bpy ligands, the Ru centered inherent stereogenicity makes it hard to get pure compounds [20]. This synthetic difficulty disappears for Ru-terpyridyl compounds, but the terpyridyl compounds of Ru are photophysically not so appealing due to the very low excited state lifetime (for Ru(terpy)$_2^{+2}$, τ = 0.25 ns) at room temperature [21]. The rigid tridentate moiety of terpyridine results in a distorted octahedral geometry in their Ru(II) complexes. In coordinated terpyridine, the N–Ru–N trans angles reduce to 158.6° from 173.0° in the analogous Ru(II)bpy complexes [22,23]. Hence the ligand field strength weakens, reducing the energy of the d–d metal-centered triplet state (^{3}MC) [24]. Consequently the energy gap between the ^{3}MLCT and ^{3}MC states decreases and thus the ^{3}MC state becomes thermally accessible from the ^{3}MLCT state, causing easy non-radiative decay back to the ground state. For a better excited state property

* Corresponding authors. Tel.: +91 33 2668 4561/4563x514; fax: +91 33 2668 2916 (J. Datta). Tel.: +91 651 2276 531; fax: +91 651 2276 052 (S. Naskar).
E-mail addresses: jayati_datta@rediffmail.com (J. Datta), subnaskar@yahoo.co.in (S. Naskar).

http://dx.doi.org/10.1016/j.poly.2015.10.040
0277-5387/

of the sensitizer, thermal non-radiative deactivation from the ^{3}MC state should be minimised. This can be achieved either by destabilizing the ^{3}MC state or by stabilizing the ^{3}MLCT state. Proper substitution (electron withdrawing or/and electron donating group) at the para position of the central pyridine ring of the terpyridine can achieve the desired effect [25]. The ^{3}MLCT state can be stabilised by introducing an electron withdrawing group at the para position of the central pyridine of the terpyridine ligand [26,27], whereas an electron donating group cannot destabilise the ^{3}MC state to a great extent [28]. Nevertheless, presence of a phenyl substituent at the para position stabilises the ^{3}MLCT state more than the ^{1}MLCT state [29,30].

Approaches have been made to develop thiocyanate free Ru dyes in order to improve the light absorption capacity as well as to avoid the possibility of getting a mixture of products due to the ambidentate nature of the thiocyanate ligand. One methodology in this respect is to use a cyclometallating ligand [31–33], which fulfills both purposes. Another approach that may be used is to change the ancillary ligand [34]. Substitution of SCN by Cl red shifts the MLCT band by 20–30 nm.

Pioneered by Professor Michael Gratzel, these ruthenium polypyridyl complexes are widely used as photosensitizer dyes in wide band gap solar cells. The most efficient photosensitizer to date is N719, with an efficiency of 11.18% [35]. Based on the above approach, we report a new Ru-polypyridyl complex (Fig. 1) which consists of a substituted terpyridine ligand, an anchoring group, 2-(2-pyridyl)-4-carboxyquinoline, and an ancillary Cl ligand. We were successful in our attempt to modulate the energy gap between the d^6-π HOMO and the ligand based LUMO by red shifting the MLCT absorbance maxima up to 536 nm using Cl as an ancillary ligand. The coordinated Cl reduces the $d\pi \rightarrow \pi^*$ energy gap and therefore causes a significant red shift in the MLCT absorbance [36]. For the majority of terpyridine based Ru complexes the low energy MLCT absorbance remains below 500 nm [34,37,38], whereas the complex reported here exhibits the MLCT absorbance at 536 nm. Here, we have used a pyridine ligand and a quinoline based anchoring group, 2-(2-pyridyl)-4-carboxyquinoline, for the dye. The anchoring group in this dye is quite non-conventional as there are no reports, to our knowledge, where such a pyridine-quinoline moiety has been used as the linker group. The extended aromatic heterocycle in this ligand may help in better delocalisation of the electron density involved in the metal to ligand charge transfer (MLCT), thus helping in better electron injection in the conduction band of TiO_2. The presence of only one –COOH linker site may seem counterproductive, but merely increasing the number of linker groups does not always enhance the efficiency of the solar cell. It has been reported that although black dye has three potential COOH linkers, it attaches to the semiconductor surface via only one carboxylic acid group due to steric congestion [39]. Our aim was to get rid of this stereochemical congestion for the attachment of the dye to the semiconductor as well as to study the electrochemical and photovoltaic behaviour of this new heteroleptic Ru complex with a new anchoring moiety. There is a possibility that these new dye molecules will be better attached on the semiconductor surface.

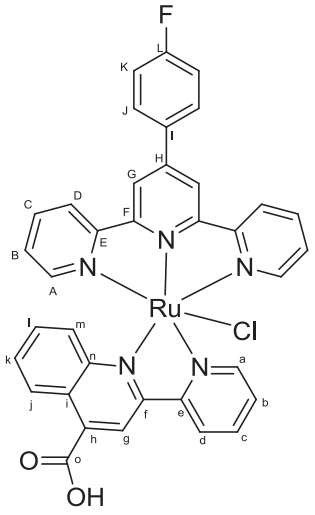

Fig. 1. Labeled structure of [Ru(*p*-F-tpy)(pcqH)Cl]PF_6.

We have also studied the spectroscopic and electrochemical properties of the dye by varying the pH from 0.04–13.17. It has been shown that both the MLCT and redox properties can be significantly tuned by changing the pH. Also an interesting observation is that the Ru–Cl bond is labile in aqueous media [34,40] and gets substituted by H_2O molecules in acidic media (within pH 4). This can provide an idea about the optimal conditions required for dye stability and effective dye regeneration for this class of photosensitisers in Dye Sensitized Solar Cells (DSSCs).

2. Experimental

2.1. Materials and methods

4-F-benzaldehyde, 2,3-indolinedione, tetrabutyl ammonium bromide and silver nitrate were purchased from Spectrochem, 2-acetylpyridine and ammonium hexafluoro phosphate were purchased from Sigma Aldrich and ruthenium chloride was obtained from Arora Mathey India Limited. The ethanol and DMF used were HPLC grade, whereas methanol was dried according to literature procedures [41]. The water used for the spectrophotometric and electrochemical studies was purified by a Milli-Q system. Tetrabutyl ammonium perchlorate was synthesised according to the literature [42].

Infrared spectra were recorded as KBr pellets on a Shimadzu IR-Prestige21 spectrometer. UV–Vis spectra were recorded using a Perkin Elmer Lambda 750 spectrophotometer. The pH values were measured in a Thermos Scientific Orion 4 star pH Benchtop. Thermogravimetric analysis of the dye was executed in a DTG-60 (Shimadzu Corporation, Kyoto, Japan) from 30 to 800 °C in a platinum pan at a heating rate of 10 °C per minute under flowing N_2 (30 ml per min.). Cyclic and differential pulse voltammograms were recorded in a CHI6003E potentiostat, either in DMF or DMF-water solutions, containing 0.1 M TBAP as a supporting electrolyte, with glassy carbon as a working electrode, a Pt wire as a counter electrode and an Ag/AgCl non-aqueous reference electrode. The ferrocene/ferrocenium couple was observed at E^0 (ΔEp) = 0.4 V (100 mV) under these experimental conditions. ^{1}H NMR spectra were recorded on a Bruker AVANCE DPX 400 MHz spectrometer using $Si(CH_3)_4$ as an internal standard. ESI-MS spectra of the samples were recorded on a JEOL JMS 600 instrument. Fluorescence spectra at room temperature were recorded using a Shimadzu RF-5301 PC spectrofluorometer.

2.2. Synthesis

2.2.1. Preparation of the ligands

2.2.1.1. 4′-(p-Fluorophenyl)-2,2′:6′,2″-terpyridine (p-F-tpy). The terpyridyl ligand has been synthesized by following the reported procedure [43]. 4-F-benzaldehyde (0.620 g, 5 mmol) and 2-acetylpyridine (1.21 g, 10 mmol) were dissolved in ethanol. KOH (0.77 g, 10 mmol) was added and the mixture was vigorously stirred. After the potassium hydroxide pellets completely dissolved, ammonia (excess, ca. 20 ml) was added and the mixture was stirred at room

temperature for 16 h under a N_2 atmosphere. The resulting solution was filtered under vacuum and washed with ethanol to give a very light blue colored fluffy solid, yield 0.656 g (40%). The crude product was recrystallised from methanol. Mass: 328 (M+1). ^{1}H NMR ($CDCl_3$, δ, ppm): 8.61 (2H, d, Ph3,5-H), 8.59 (2H, d, Ph2,6-H), 8.55 (2H, d, 6,6"-H), 7.75 (2H, ddd, 5,5″-H), 7.8 (2H, ddd, 4,4″-H), 7.15 (2H, s, 3′,5′H), 7.05–7.1 (2H, m, 3,3″-H). ^{13}C NMR ($CDCl_3$, δ, ppm): 155.76 (C_L), 154.80 (C_F), 149.34 (C_E), 148.19 (C_H), 137.47 (C_A), 136.29 (C_C), 134.35 (C_I), 129.36 (C_J), 128.78 (C_B), 124.38 (C_D), 120.94 (C_G), 117.82 (C_K).

2.2.1.2. 2-(2-pyridyl)-4-carboxyquinoline (pcqH). This ligand was prepared according to the literature method [44]. 18 g (0.12 mol) of 2,3-indolinedione was crushed to a powder and mixed with 15 g (0.12 mol) of 2-acetylpyridine for ~30 min. 60 g (~60 ml) of 33% NaOH were added at 5 °C with stirring. The solution was stirred continuously for 30 min, whereupon the temperature raised to ~50 °C. Ice flakes were added to the mixture. Stirring the mixture with a glass rod produced a purple red solid. The solid was filtered, washed with water followed by cold acetone. The crude product was recrystallised from water to give a light purple crystal. Yield: 18 g (67%) Mass: 295 (M+23+23) (base peak) (23 = mass of Na^+).

2.3. Preparation of the complexes

2.3.1. Ru(p-F-tpy)Cl$_3$

p-F-tpy (1.2 g, 3.67 mmol) and $RuCl_3$ (0.95 g, 3.67 mmol) were dissolved in 20 ml dry methanol and heated to reflux under N_2 for 3 h. The resulting deep brown solution was allowed to cool at room temperature, after which the solution was cooled in an ice bath for 0.5 h. The brown solid that formed was collected by vacuum filtration and washed with cold methanol until the filtrate was colorless, and then it was washed with Et_2O and air dried. The product (yield: 0.691 g, 35.24%) was used without further purification.

2.3.2. [Ru(p-F-tpy)(pcqH)Cl](PF$_6$) (**1**)

Ru(*p*-F-tpy)Cl_3 (0.267 gm, 0.5 mmol) and pcqH (0.125 gm, 0.5 mmol) were taken in a round bottomed flask in 25 ml dimethyl formamide (DMF) and refluxed for 6 h under N_2. The reaction mixture solution was then reduced in rotary evaporator to 5 ml and a saturated aqueous solution of NH_4PF_6 was added to the solution. On addition of more water, a precipitate appeared, which was collected by filtration in a G4 sintered glass filter. Yield: 0.346 g, 84.18%. The product was purified by column chromatography using silica as the stationary phase and DCM as the mobile phase. The violet colored product (0.088 g, 22.5%) was eluted with 1:1 DCM/CH_3OH eluent. ESI-Mass, *m/z*: 712.5.

^{1}H NMR (d-6 DMSO, δ, ppm): 10.3 (1H, d, H_a), 9.15 (1H, d, H_j), 9.04 (1H, d, H_g), 8.86 (4H, d, H_G, H_D), 8.6 (2H, s, H_K), 8.42 (1H, dd, H_b), 8.35 (1H, d, H_d), 8.3 (1H, m, H_m), 8.00 (2H, m, H_C), 7.60 (2H, m, H_A), 7.56 (2H, d, H_J), 7.50 (1H, m, H_l), 7.35 (2H, m, H_B), 7.30 (1H, d, H_k), 7.1 (1H, m, H_c). ^{13}C NMR (d-6 DMSO, δ, ppm): 164.698 (C_o), 162.232 (C_L), 158.699 (C_F), 158.485 (C_E), 153.062 (C_e), 152.707 (C_f), 151.774 (C_H), 151.889 (C_A), 150.447 (C_a), 137.403 (C_n), 137.031 (C_C and C_c), 136.786 (C_l), 130.565 (C_h), 130.130 (C_l), 128.114 (C_m), 127.632 (C_k), 127.427 (C_K), 126.549 (C_g), 126.454 (C_b), 126.020 (C_J), 124.478 (C_D), 124.280 (C_d), 123.814 (C_i), 120.099 (C_B), 116.352 (C_G), 116.130 (C_j).

2.4. TiO$_2$ paste and thin film preparation

TiO_2 paste was prepared in the laboratory using nanocrystalline grade TiO_2 powder, acetic acid, de-ionized water and surfactants [45]. The nano-crystalline TiO_2 paste was applied as a thin film over FTO glass plates (Fluorine doped tin oxide on one side making it electrically conducting) using a glass rod with quick downward sweeping motions by the Doctor's Blade technique, the cell area being maintained at 0.5 cm^2. The films were made fairly smooth, avoiding any inconsistencies or streaks in the applied TiO_2 paste. The thickness of the film (≈14–15 μm) was gravimetrically measured using a highly sensitive digital micro-balance, Metler-Toledo [Model No.AB265-S], Switzerland and further verified with a Mitutoyo ABSOLUTE (No. 547-301) thickness meter. In order to dry and strengthen the TiO_2 coating, the coated plates were sintered at 500 °C for ~30 min, until a transformation from white to a brownish colour and back to white again took place. Finally the TiO_2 thin films were cooled to room temperature and made ready for dye sensitization.

2.5. Fabrication of the Dye Sensitized Solar Cell

In order to form the photo-anode, the thin films of TiO_2 were sensitized with the synthesised dye (**1**) and a reference dye (N719) by immersing the films overnight in a 1 mM ethanolic solution of the appropriate dye. The counter electrode of the proposed DSSC cell was prepared by galvanostatic electro-deposition of Pt nanoparticles onto the FTO glass substrate from a precursor H_2PtCl_6 solution, applying a current density of 5 mA cm^{-2} for 300 s. The two electrodes were assembled together using Bynel (SX1170-60, 50 μm thick, Solaronix) as the sealant, heating at ~80 °C. Subsequently, the working electrolyte, composed of 0.5 M NaI (Sigma–Aldrich), 0.05 M I_2 (Sigma–Aldrich), 0.05 M TPMPI (Triphenylmethylphosphonium iodide effectively used in low light ambience [46]) and 0.5 M 4-tertbutyl pyridine (TBP, Sigma–Aldrich) in acetonitrile [47], was injected into the cell system and the cell was sealed properly. It may be noted that in the I_3^-/I^- redox electrolyte, TBP acts as an important additive by improving the open circuit potential (Voc) of the cell [48]. It has been further reported that TBP increases the electron lifetime in the TiO_2 conduction band thereby arresting the recombination effect. The fabricated DSSCs were subjected to performance screening with the help of electrochemical techniques.

2.6. Electrochemical impedance spectroscopy (EIS)

In order to determine the charge-transfer resistance and double layer capacitance across the dye-sensitized semiconductor electrode – redox electrolyte interface, the fabricated DSSC cells were subjected to EIS measurements at room temperature with the help of AUTOLAB 302 N PG-stat, Eco-Chemie BV (The Netherlands) combined with the NOVA-v1.10 software package, under background illumination from a high-power white light emitting diode (LED). The frequency dispersion impedance spectra (Nyquist plot) for the DSSC cells were recorded by applying a sinusoidal perturbation of 5 mV amplitude at the working electrode over a frequency range of 100 kHz to 10 mHz at the respective open circuit potentials and under illumination of 30 mW/cm^2 measured with an optical powermeter (Newport, 1916-R, Canada).

2.7. I–V characteristics, transient photoresponse and incident photon-to-current conversion efficiency (IPCE) records

Performance output of the DSSC cell was derived in terms of photo-conversion efficiency with the help of current–voltage (*I–V*) measurements under a light intensity of 30 mW cm^{-2} from a white LED light source. The photoresponse of the films, in terms of rise and decay of the short-circuit current (I_{sc}) at 20 s intervals in the dark and illuminated conditions, was recorded with a similar cell setup. IPCE spectra of the cells were recorded with a xenon lamp light source using a grating monochromator (Sciencetech 9055, Canada).

2.8. Computational details

The quantum chemical calculations were performed using density functional theory (DFT) implemented in GAUSSIAN 09 [49]. A split basis set was used for the optimization of the complex using the B3LYP hybrid functional and 6–31 g (d) basis set for hydrogen, carbon, oxygen, nitrogen and fluorine atoms and the LANL2DZ basis set for the ruthenium atom. The absorption spectra were simulated using Time Dependent Density Functional Theory (TD-DFT). All the computational studies were carried out in DMSO solvent using the Polarizable Continuum Model (PCM) implemented in GAUSSIAN 09. The orbital contribution was calculated by GaussSum [50].

3. Results and discussion

3.1. Synthesis

The synthesis of the novel complex [Ru(*p*-F-tpy)(pcqH)Cl]PF_6 (**1**) (F-TPY = 4′-(4-fluoro phenyl)-2,2′:6′,2″ terpyridine, pcqH = 2-(2-pyridyl)-4-carboxyquinoline) has been outlined in Scheme 1. The ligands *p*-F-terpyridine and 2-(2-pyridyl)-4-carboxyquinoline have been synthesized according to the published procedures.

The ruthenium complex has been synthesized first by the reaction of the terpyridine ligand with $RuCl_3$ in dry methanol for 3 h and then, after subsequent washing with cold methanol and filtration and drying of the solid formed, by further reaction of this solid with the anchoring group (pcqH) in DMF for 6 h. The product was precipitated by treatment with excess NH_4PF_6 and addition of water to a reduced volume of the DMF mixture. The solid so obtained was filtered, dried and further purified by column chromatography in silica, where the desired complex was eluted by 40–50% methanol in dichloromethane as a deep reddish violet coloured solution. The molecular structure has been characterised by mass and NMR spectroscopy. There is the possibility of the formation of two isomers for the molecule, depending upon the coordination of the pcqH ligand; the pyridine or quinoline N atom trans to the central pyridine of *p*-F-tpy. In the present case we get the isomer where the pyridin-N atom of pcqH is present at the trans position of central pyridine ring of *p*-F-tpy. This has been confirmed by both the DFT optimized structure and the ^1H NMR spectrum of the complex. The H atom at the ortho position of the pyridine-N atom (H_a in Fig. 1) of pcqH remains close to Cl. Consequently the signal for H_a is shifted to higher field (δ = 10.3 ppm) than the other aromatic protons. Similar observations have been reported by D.J. Wasylenko et al. [40].

3.2. Thermogravimetric analysis

Thermogravimetric analysis of the dye **1** was monitored in the range 30–800 °C to measure the thermal stability of this new dye. As seen in the thermogram (Fig. 2) the atmospheric moisture absorbed in the dye is removed by 60 °C. There is no weight loss up to 216 °C, when carbon dioxide elimination starts and this gets completed at 300 °C. Thereafter the compound starts to decompose on further heating. The thermogram thus clearly indicates that the dye is fairly stable up to 216 °C.

3.3. Absorption spectra

In DMSO, complex **1** shows two intense ligand centered bands at 277 and 321 nm in the UV region (Fig. 3a). As per the literature [51], these peaks may also have a contribution from a high energy MLCT band arising from a Ru to p-F-tpy/pcqH ligand transition. There is also a moderately strong low energy MLCT band at 536 nm (Fig. 3c).

The absorption spectra of the complex **1** (Fig. 3b) have been studied at various pH values (0.04–13.17). At pH 0.04 the complex exhibits a MLCT band at 547 nm. With an increase in pH, the energy of the MLCT band increases and appears at 522 nm at pH 3.54. The position of the band remains constant at 522 nm up to a pH value of 11.27. On further increasing the pH value, the MLCT band is red shifted to 527 nm at pH 13.17.

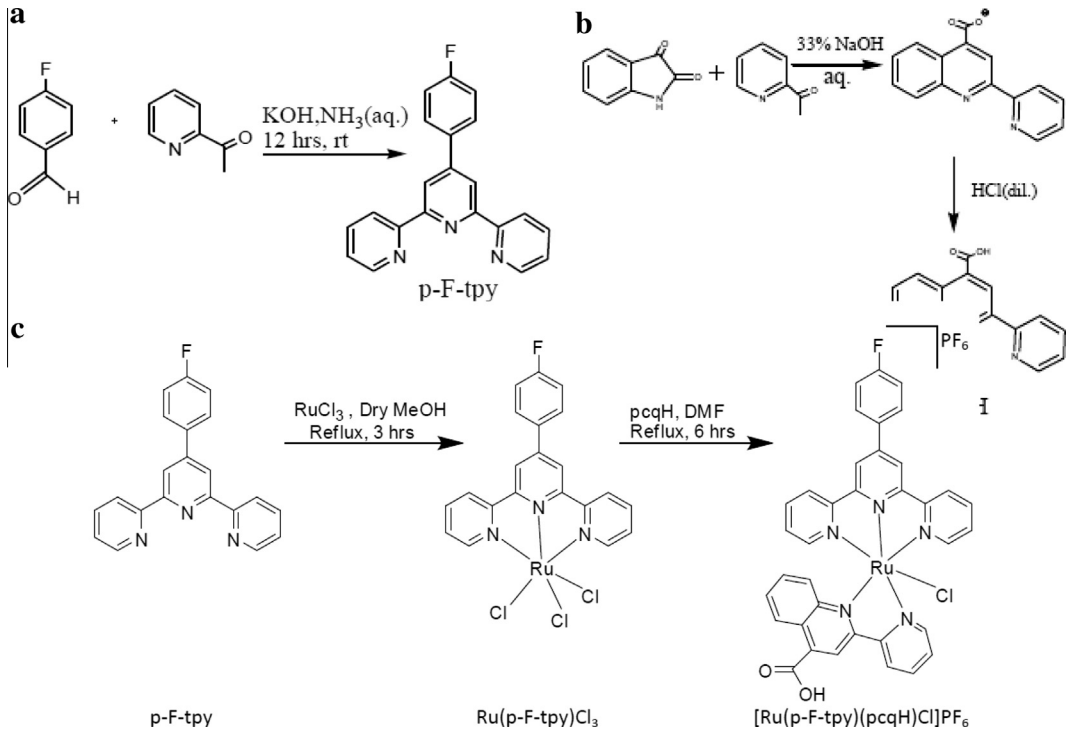

Scheme 1. Synthetic routes for (a). *p*-F-tpy (b) pcqH (c) [Ru(*p*-F-tpy)(pcq)Cl]PF_6.

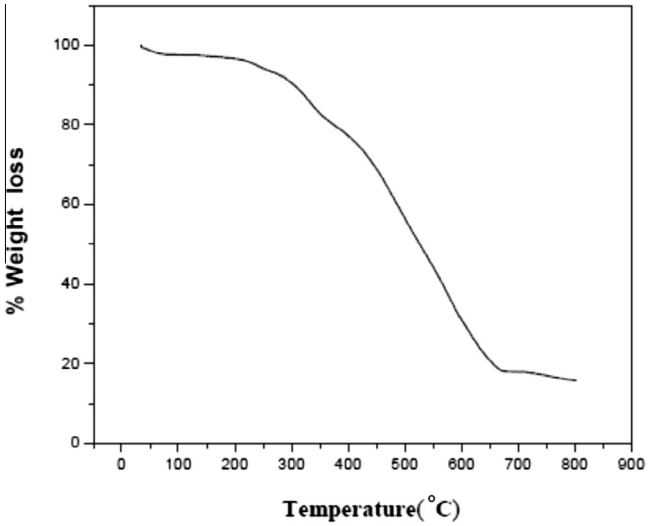

Fig. 2. Thermogram of the dye [Ru(*p*-F-tpy)(pcqH)Cl]PF_6.

At pH 0.04, the carboxylic acid of pcqH remains protonated. Deprotonation of the –COOH group takes place within the pH window of 1.56–3.54, evident in the large blue shift of the MLCT peak position from 547 to 522 nm. This blue shift of 25 nm may be due to the combined effect of -COOH deprotonation [52] as well as replacement of Cl by H_2O. The former destabilizes the π^* orbital in pcq^- while the later stabilises the dπ (Ru) orbital. It has already been reported that the Ru–Cl bond is not robust in aqueous medium. This in-situ formed aqua complex is stable up to pH 11.27. An interesting feature in the plot of absorbance at fixed wavelength versus pH is the appearance of a 2nd inflection point after pH 11.27. This later inflection point marks the deprotonation of the coordinated H_2O that replaced the Cl ligand. In highly alkaline medium, conversion of H_2O to OH^- again increases the energy of the t_{2g} orbital of Ru due to the stronger π donor property of OH^-. Similar results have been reported by Wrighton et al. [53] and M. Gratzel et al. [34]. A change in the MLCT band position with the variation of pH value is also reflected by the naked eye colour change of the complex. The colours at pH 0 and pH 13 are more intense than those at the other pH values (Fig. 4).

3.4. Spectrophotometric determination of pK_a values

The pK_a values of the Ru complex **1** were determined by spectrophotometric titration. The ground state pK_a values can be determined by plotting the change in absorbance with pH at a fixed wavelength. 1.4×10^{-3} M TBAP (tetrabutyl ammonium perchlorate) was added to maintain the ionic strength of the solution. The spectrophotometric titration of the complex shows interesting features.

A 200 ml 7×10^{-5} molar solution (1:1 DMF-H_2O) of complex **1** was prepared for the spectrophotometric titration. The pK_a values were obtained from the inflection point of the plot for absorptions at 285, 315 and 516 nm versus pH (Fig. 5). From all the three plots, two clear inflection points were obtained at 2.89 and 12.20. The former is assigned to be the deprotonation of the –COOH group of pcqH, while the later may be due to the deprotonation of the water molecule attached to Ru that replaced the Cl ligand during the addition of aqueous NaOH. The pK_a value of the coordinated H_2O molecule has been previously reported by Mayer [54,55] and Gratzel [34]. The pK_a values increase with an increase in the basicity of the spectator ligand. The presence of a $-COO^-$ group in the molecule increases the basicity of the H_2O ligand to 12.20.

3.5. Electrochemical studies

Cyclic voltammetry (Fig. 6) of the Ru complex (**1**) in DMF medium shows a reversible oxidation wave at 0.85 V with $i_a/i_c \sim 1$ and $\Delta E_p = 70$ mV. In the cathodic scan the complex shows a quasireversible reduction process at −0.96 V and two additional peaks at −1.56 and −1.73 V. Cyclic voltammetry of the free ligands (Fig. 7) shows similar reduction process: pcqH (−1.01 V), 4F-terpy (−1.14, −1.79 V). Therefore, on the cathodic side the reduction of the complex may be due to a ligand based electron transfer. The reversibility of the oxidation process of complex **1** is verified by the constant $E_{1/2}$ value at different scan rates (20–500 mV/Sec) (Fig. 8a) as well as from the plot of $i/(v)^{1/2}$ versus v, (where i = current and v = scan rate) (Fig. 8b).

The detailed redox properties of complex **1** were studied by means of cyclic voltammetry and differential pulse voltammetry at variable pH (0–13) (**SM7**). The complex exhibits pH dependent redox behavior. Throughout the whole pH range on the anodic side one reversible couple is observed in the range 0.44–0.87 V (E_I^0), whereas in the pH range 6.08–6.53 a second reversible peak (E_{II}^0) is obtained at 0.91 V. The first oxidation wave (E_I^0) shows pH dependence in the range 6.08–11.36, but the second reversible electron transfer process (E_{II}^0) is independent of pH. Here we assign the first reversible peak as $Ru^{II/III}$ and the second peak as the $Ru^{III/IV}$ oxidation process.

At pH 0, the –COOH group of the anchoring ligand remains protonated. The spectrophotometric titration shows that the

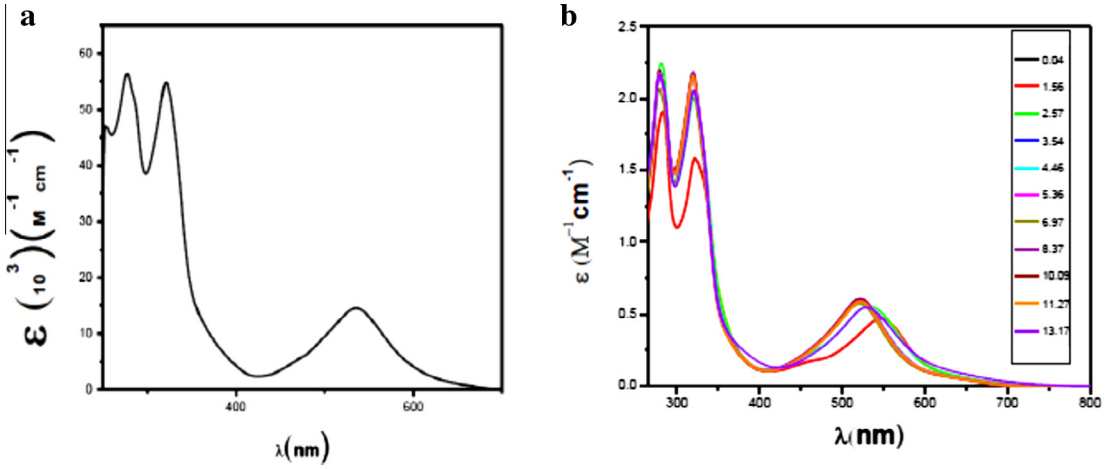

Fig. 3. Absorbance spectra of (a) [Ru(*p*-F-tpy)(pcqH)Cl]PF_6 in DMF (b) [Ru(*p*-F-tpy)(pcqH)Cl]PF_6 in (1:1) DMF:H_2O in the pH range 0.04–13.17.

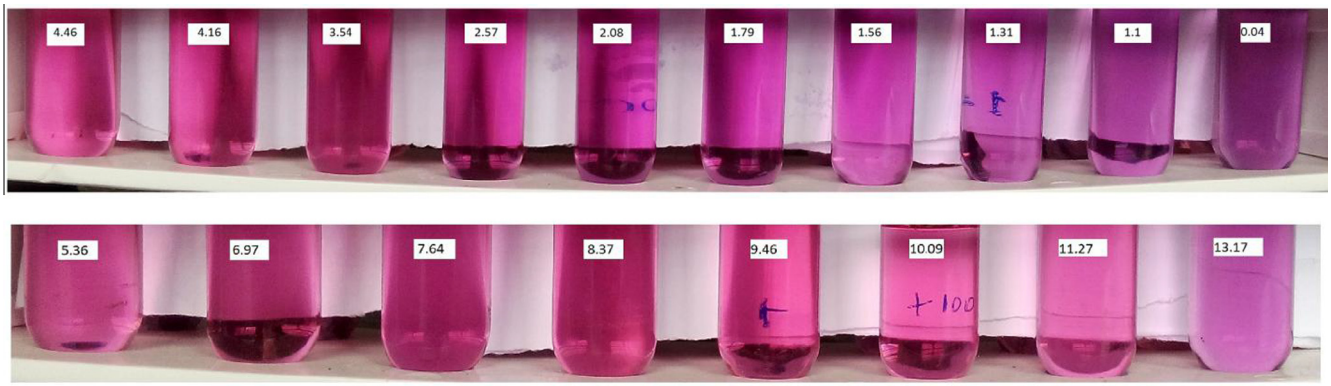

Fig. 4. DMF-H_2O (1:1) solution of the dye ([Ru(*p*-F-tpy)(pcqH)Cl]PF_6) at different pH.

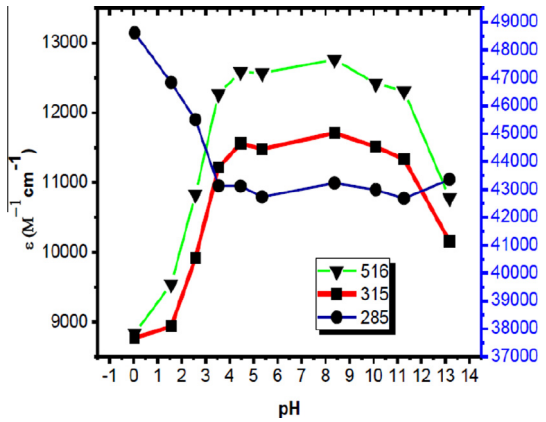

Fig. 5. Absorptivity vs. pH at 516 nm, 315 nm and 285 nm of the complex ([Ru(*p*-Ftpy)(pcqH)Cl]PF_6).

deprotonation of the –COOH group has a pK_a of 2.89. The E_l^0 value continuously increases from pH 0 to 4.31. With the increase in pH from 0 to 4.31 two process simultaneously operate: deprotonation of the –COOH group and the replacement of the Cl ligand by a water molecule. Formation of $–COO^-$ increases the electron density on the Ru atom, reducing the E_0 values, while replacement of Cl by H_2O reduces the electron density on the Ru atom and increases the E_0 values. Since H_2O is directly connected to Ru, H_2O addition dominates the deprotonation of the –COOH group. Consequently the redox potential increases. After pH 6.08, the potential gradually decreases up to pH 11.36. So in this range the redox process is pH dependent. Water is deprotonated to OH^-. Therefore the process may be assigned as a proton coupled electron transfer. On further increasing the pH, the E_0 value remains constant. Hence the redox process is independent of pH.

The complete redox behavior of the Ru complex **1** is shown by the Pourbaix diagram (Fig. 9a). The molecule contains two acidic protons in -COOH and H_2O. So two different proton coupled electron transfer process are expected. In the pH range 0–4, since the deprotonation of –COOH is accompanied by the removal of Cl by H_2O, the expected trend in $E_{1/2}$ for THE $Ru^{II–III}$ oxidation is not obtained experimentally. This could only be achieved by starting with an aqua complex instead of the Chloro complex (**1**). The Pourbaix diagram displays experimental $E_{1/2}$ versus pH graph within the pH range 4–13. In the pH range 4–6.25, two chemically reversible species, $Ru^{II}H_2O$ and $Ru^{III}H_2O$, exist. This process is independent of pH. From pH 6.25–11.36 the two species are $Ru^{II}H_2O$ and $Ru^{III}OH$. A 2nd redox process appeared in anodic side of the CV in the range pH 6.08–6.53 at a relatively high potential (0.905 V). This may be due to the $Ru^{III/IV}$ oxidation.

The relation of $E_{1/2}$ with pH can be expressed by the following equations [56] where $E^0_{1/2}$ is the standard redox potential of the $Ru^{II/III}$ couple at pH 4.31; α_{red} is the concentration of the reduced species and α_{ox} is the concentration of the oxidised species, K_1 is the H_2O deprotonation constant in the Ru^{II} state and K_2 is that in the Ru^{III} state (Scheme 2).

$$E_{1/2} = E^0_{1/2} + (RT/F)\ln(\alpha_{red}/\alpha_{ox})$$

where $\alpha_{red} = 1K_1/[H]^+$

$\alpha_{ox} = 1 + K_2/[H]^+$

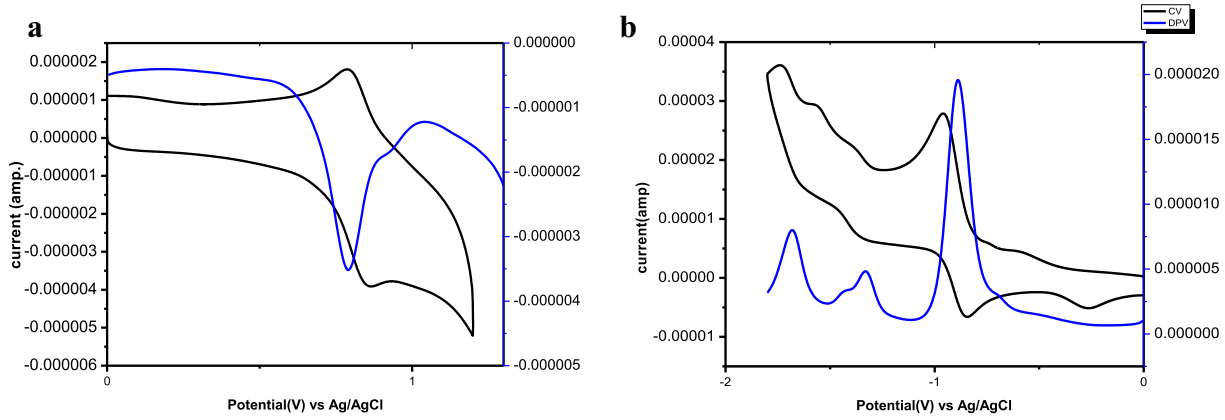

Fig. 6. Cyclic voltammetry and differential pulse voltammetry in DMF solvent of [Ru(*p*-Ftpy)(pcqH)Cl]PF_6 at a scan rate of 100 mV/s of (a) anodic side (b) cathodic side.

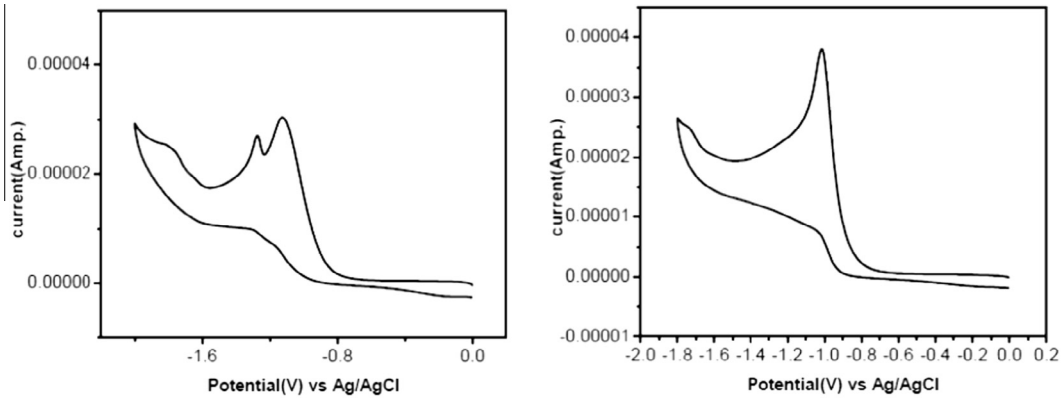

Fig. 7. Cyclic voltammetry (Cathodic Scan) of p-F-tpy (left) and pcqH (right) in DMF.

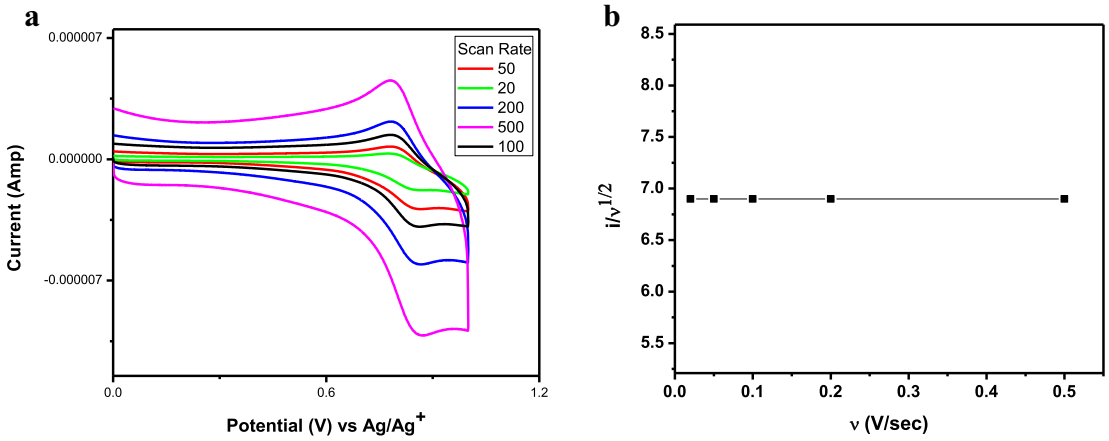

Fig. 8. (a) Cyclic voltammetry of [Ru(*p*-F-tpy)(pcqH)Cl]PF_6 at different scan rates and (b) $i/v^{1/2}$ vs. v (scan rates).

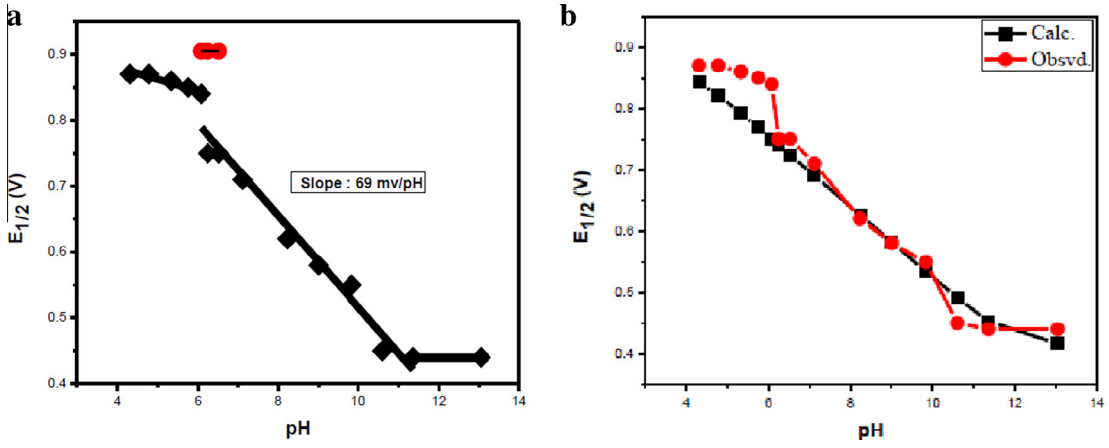

Fig. 9. (a) Pourbaix diagram ($E_{1/2}$ vs. pH) of [Ru(*p*-F-tpy)(pcqH)Cl]PF_6 and (b) plot of calculated and observed $E_{1/2}$ vs. pH for [Ru(*p*-F-tpy)(pcqH)Cl]PF_6.

Non-linear regression analysis (Fig. 9b) by using the Microsoft Excel Solver program was done according to the above equations to generate pK_a values for Ru^{II} as 11.89 (pK_1) and for Ru^{III} as 4 (pK_2).The pK_1 value conforms to the pK_a value obtained from the acid-base spectrophotometric titration (pK_1 = 12.20). The decrease in the pK_a value by almost 8 units upon changing from the Ru^{II} to Ru^{III} state for the aqua ligands in a polypyridylic type of complex is in accord with the literature [57].

3.6. Photovoltaic study

The anchoring group in this dye with a single carboxylic acid is quite unconventional. It has been reported [58] that the black dye, despite having three potential COOH linkers, attaches to the semiconductor surface via only one carboxylic acid group due to steric congestion. Therefore, there exists a fair possibility of the dye molecule (**1**) to get better attached on the semiconductor surface

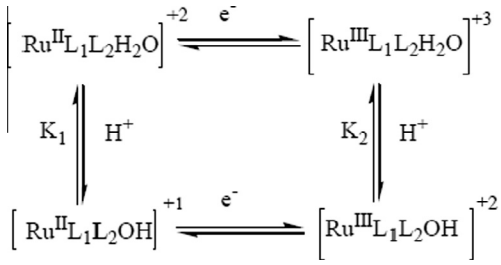

Scheme 2. Outline of the electrode process for the Ru^{III}–Ru^{II} couple, involving both redox and acid–base equilibria.

[59–61], creating more reaction sites and enhancing the absorption capability of the matrix.

The functional properties like Voc, short-circuit current density (Isc), fill factor (FF) and solar-to-electrical conversion efficiencies (η) were derived for the fabricated DSSCs, employing the respective electrochemical techniques. The power output characteristics of **1**-TiO_2 and N719-TiO_2 based DSSCs are presented in Fig. 10. In the case of **1**-TiO_2 matrices the Voc values and percent efficiency are rather compromised compared to those of N719-TiO_2 based DSSC (inset). However, even with a moderate photon to energy conversion efficiency of 0.13%, **1**-TiO2 exhibits a fill factor of 39.4%, which is promising.

The impedance spectra (Fig. 11) of the films at the respective open circuit potentials (OCP) were recorded for the cell configuration FTO/TiO_2/**1**/I^{3-} – I^-/Pt–FTO and were further analyzed based upon the simple equivalent circuit (EC) model constituting several circuit components. The circuit included a solution resistance (R_s), charge transfer impedance (R_{ct}) and a constant phase element (Q) as the non-ideal capacitor, which substitutes the double layer capacitance of the electrode–electrolyte interface and Warburg impedance [30]. It has been observed that the cell exhibited high charge transfer resistance (5.71 kΩ) and moderate values of the constant phase element (Q) (4.87 h), whereas N719 based DSSC shows charge transfer resistance (73.1 Ω) with a constant phase element of 217 h (Fig. 11 inset). This may be rationalized due to the presence of a lower number of anchoring groups in the sensitizer **1**.

In Fig. 12 an instantaneous photo response is featured with the rise and decay curves of photocurrent density (Isc) during successive exposure of the films to illuminated and dark conditions. The overall photoresponse behaviour of such type of unconventional dye in the device is much more than expected and can also be modified by extending the anchoring site through a preferable

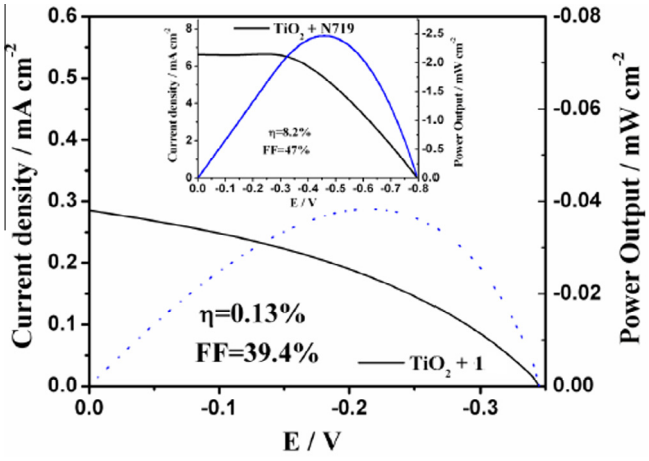

Fig. 10. Current–voltage and power output characteristics, measured in 0.3 AM white LED illumination for a DSSC using 1 and N719 (Inset) as the molecular sensitizer over titania matrix respectively.

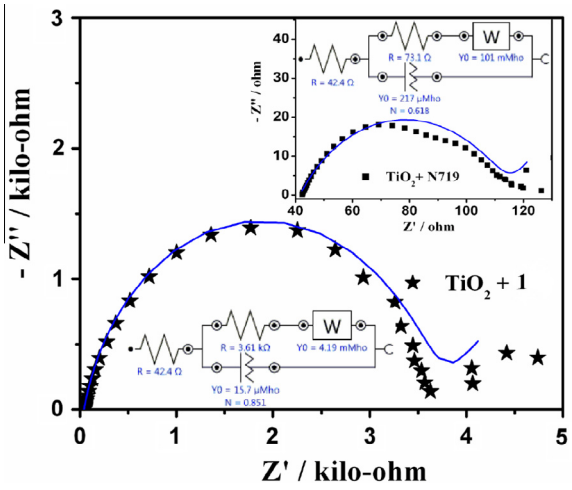

Fig. 11. Nyquist plot of the dye 1 and N719 dye (Inset) sensitized DSSC system, scanned from 105 to 0.1 Hz.

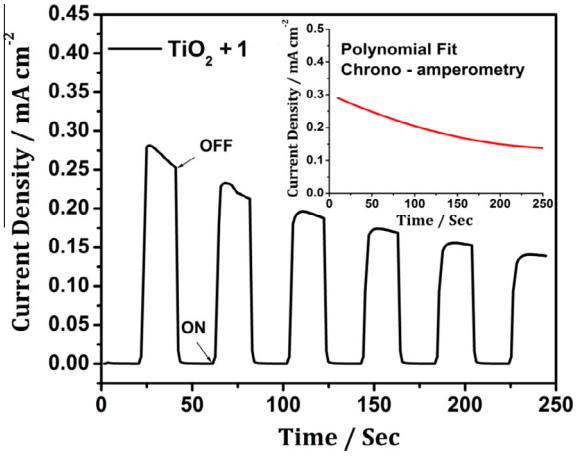

Fig. 12. Short-circuit current density (Isc) – rise and decay curves for the cell system FTO–1- /I3–I –/ Pt–FTO. Inset shows polynomial fit chrono-amperometric plot.

group. The inset figure depicts the chrono-amperometric study through a polynomial fit over a specified time barrier. The slow decay indicates that the stability of the **1**-TiO_2 based DSSC device is also satisfactory.

The IPCE measurement provides information about the absorption capability of the photo-anode and the kinetic efficiency of the electron transport during the energy conversion process. Fig. 13 shows the action spectrum of IPCEs for the **1**-TiO_2 solar cell, which is quite impressive compared to the N719 based system in the inset. In the case of the N719 sensitizer, the maximum IPCE exhibited was of the order of 52%, whereas for the dye (**1**) the IPCE attains a considerable value of 40%, which is indicative of the facile electron transfer process from the excited **1** to the conduction band of the semiconductors. It appears **1** synthesized DSSC is particularly effective in the spectral range 420–550 nm. However, the spectral responses of this new dye can be expanded with further modifications, co-sensitization in the matrix and optimizing the electrolyte composition.

3.7. DFT calculations

A computational study using density functional theory with the B3LYP hybrid functional was performed to get the optimized

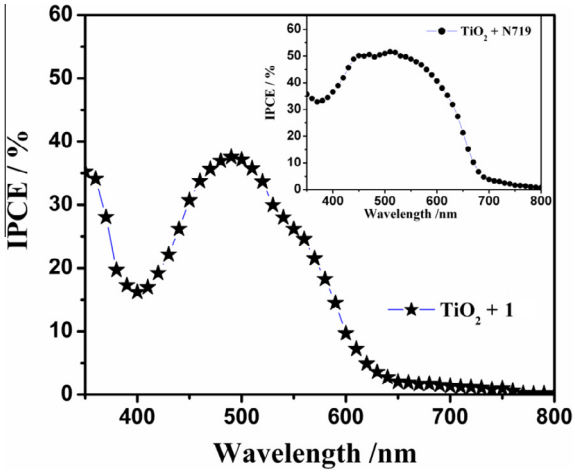

Fig. 13. Photocurrent action spectra of the 1 and N719 (Inset) sensitized DSSC device.

structures of the ligands and the Ru(II) complex in DMSO for a better understanding of their electronic structures. The compositions and energies of the frontier molecular orbitals of the complex are given in Table 1 while the metrical parameters are displayed in Table 2. The method used for the optimization is perfect, as is evident from close matching with the literature for similar molecules. The molecule adopts a distorted octahedral geometry where the cis angles vary from 77.35–106.29° and the trans angles are in the range 157.45–176.28°. Due to its rigidity, the terpyridine ligand is expected to coordinate to the metal centre in a meridional fashion, which is also observed in our optimized structure. In a number of related 4 substituted terpyridine ligands, Y. Tanaka et. al. reported the bond length for Ru-N_{py}(central) is smaller (~1.97 Å) than that of Ru-N_{py}(terminal) (~2.07 Å). In our case we also find a similar trend, where the Ru-N_{py}(central) bond length is 2.00 Å and the Ru-N_{py}(terminal) bond length is 2.11 Å [62]. A comparison with the optimized geometry of the $[Ru(bpy)(terpy)Cl]^+$ system [63] also shows a similar trend in the Ru-N_{py} distances.

The other basal coordination is made by the pyridine-N atom of the anchoring ligand, whereas the axial sides are coordinated by

Table 1
Compositions and energies of the frontier molecular orbitals of the complex.

Energy(eV)	−6.84	−6.04	−5.88	−5.74	−2.98	−2.51	−2.3	−1.82
Atom/ligand %	HOMO−3	HOMO−2	HOMO−1	HOMO	LUMO	LUMO+1	LUMO+2	LUMO+3
Ru	3	75	66	70	5	7	2	1
Cl	13	1	11	11	0	1	0	0
p-F-tpy	81	8	20	12	1	91	98	2
pcqH	3	16	3	7	93	1	1	98

Table 2
Metrical parameters of the optimized structure of the complex.

Geometry (Å, °)							
Bond	(Å)	Angle	(°)	Angle	(°)	Angle	(°)
Ru–Cl	2.49	Cl–Ru–N3	89.18	N7–Ru–N4	106.29	N5–Ru–N3	157.45
Ru–N3	2.12	Cl–Ru–N4	83.36	N7–Ru–N5	96.24	N5–Ru–N4	78.75
Ru–N4	2.00	Cl–Ru–N5	88.58	N7–Ru–N6	77.35	N4–Ru–N3	78.70
Ru–N5	2.11	Cl–Ru–N6	92.96	N6–Ru–N3	100.76		
Ru–N6	2.11	Cl–Ru–N7	169.87	N6–Ru–N4	176.28		
Ru–N7	2.16	N7–Ru–N3	89.72	N6–Ru–N5	101.76		

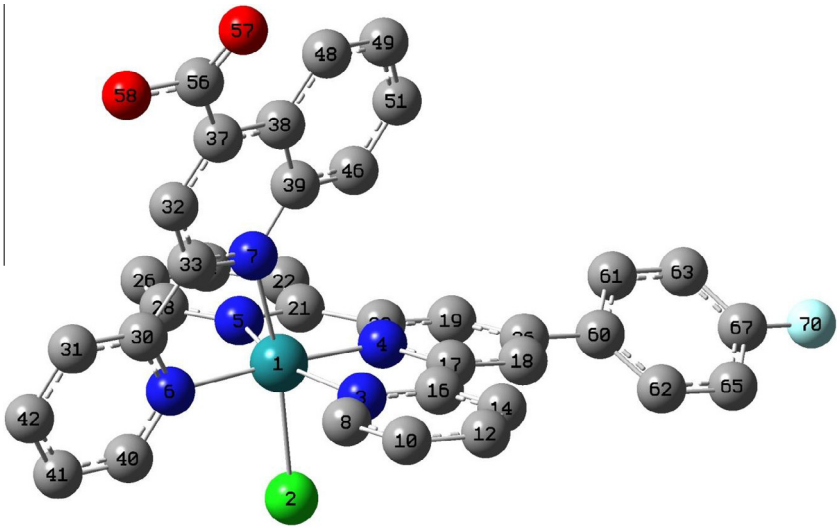

Fig. 14. DFT optimised structure of Ru[(*p*-F-tpy)(pcqH)Cl] PF_6 (**1**).

the quinoline-N atom of the anchoring ligand and the ancillary Cl ligand. A comparison with the tris chelate Ru complex of the 2-(2-pyridyl)-4-carboxyquinoline) ligand [64] also shows a similar trend in the Ru-N_{py} and Ru-$N_{quinoline}$ bond distances. Literature values for the two bonds are 2.06 and 2.15 Å, whereas for the present molecule those values are 2.11 and 2.16 Å, respectively. The small deviation is explainable considering the crystal geometry and the structure in DMSO. Composition of the frontier molecular orbitals shows that HOMO, HOMO−1 and HOMO−2 have maximum contributions from Ru, whereas HOMO−4 is terpyridine based. On the other hand, LUMO and LUMO+3 are rich with 2-(2-pyridyl)-4-carboxyquinoline ligand character and LUMO + 1 and LUMO + 2 are mostly comprised of the terpyridine ligand. The optimized structure of the molecule is given in Fig. 14.

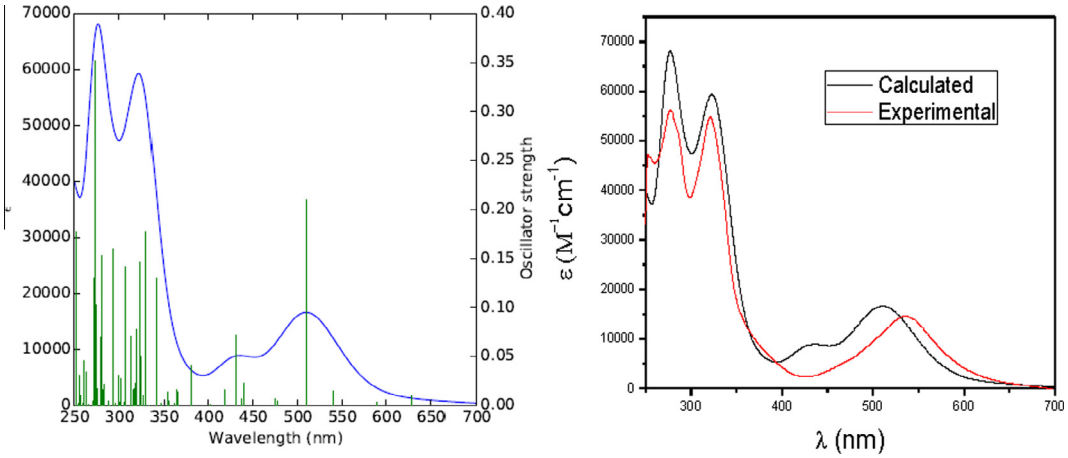

Fig. 15. The calculated UV–Vis spectrum of Ru[(*p*-F-tpy)(pcqH)Cl] PF_6 (**1**) (left) in DMSO(Green vertical lines correspond to calculated oscillator strengths) and a plot of the experimental and calculated UV–Vis spectrum in DMSO(right). (Colour online.)

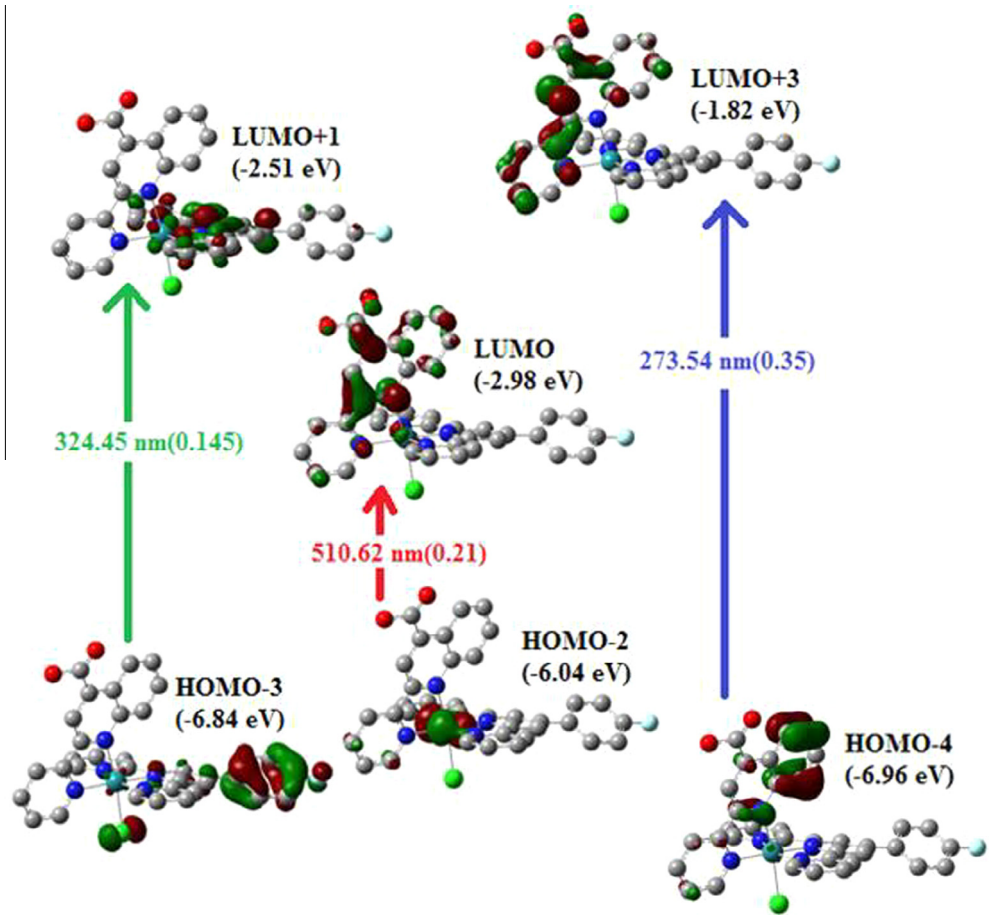

Fig. 16. Electronic transitions assigned to the major peaks.

Table 3
Vertical excitations with band position, oscillator strength (f) and character assignment.

Expt peak (nm)	Calculated peak (nm)	Oscillator strength (f)	Maximum orbital contribution	From				To				Assignment
				pcqH	*p*-F-tpy	Cl	Ru	pcqH	*p*-F-tpy	Cl	Ru	
536	510.62	0.2101	H-2->LUMO (80%)	16	8	1	75	93	1	0	5	Ru→pcqH
458	440.2	0.023	H-1->L+2 (81%)	3	20	11	66	1	98	0	2	Ru→p-F-tpy
330	330.4	0.1767	HOMO->L+5 (42%)	7	12	11	70	79	18	0	3	Ru→pcqH
321	324.45	0.1455	H-3->L+1 (88%)	3	81	13	3	1	91	1	7	p-F-tpy→p-F-tpy
288	294.04	0.1592	H-9->L+1 (61%)	4	21	66	10	1	91	1	7	Cl→p-F-tpy
271	273.54	0.3515	H-4->L+3 (31%)	89	6	3	2	98	2	0	1	pcqH→pcqH

3.8. TDDFT studies

The consensus between the computed and experimental absorption spectra in DMSO is presented in Fig. 15. The experimental peaks at 277 and 321 nm have been matched nicely with the theoretical observations at 273 ($f = 0.35$) and 324 nm ($f = 0.145$), respectively. The former band involves a pcqH centered transition while the later has been found to involve a *p*-F-tpy based electronic transition. The band at 536 nm have been computed with a slight blue shift at 510 nm ($f = 0.21$) which can be assigned a MLCT character from the Ru atom to the anchoring ligand pcqH. Moreover the shoulders accompanying all the major peaks have been calculated with great accuracy at 294 ($\lambda_{expt} = 288$), 330 ($\lambda_{expt} = 330$) and 440 nm ($\lambda_{expt} = 458$ nm). Here, an interesting observation is that the electronic transitions for the shoulder are quite different in nature from the corresponding major peaks, as observed from the simulated UV–Vis spectrum. The absorption at 277 nm is pcqH based, whereas the shoulder at 288 nm involves a transition from the ancillary Cl ligand to the terpyridine ligand. The band at 321 nm is terpyridine based, whereas the very broad shoulder at 330 nm is actually a high energy MLCT involving Ru and the pyridine moiety of pcqH. Unlike the major peak at 536 nm, a low intensity shoulder at around 458 nm, which has been observed very prominent in TDTDFT, is a MLCT from Ru to *p*-F-tpy, i.e. away from the anchoring ligand.

Hence, it can be seen that there are only two transitions where the electron density shifts towards the dye semiconductor interface through the anchoring 2-(2-pyridyl)-4-carboxyquinoline ligand. The remaining transitions are away from the linker group and serve no purpose in enhancing the probability of electron injection into the conduction band of the semiconductor. This can be one reason behind the lower efficiency of the dye. The corresponding molecular orbitals (shown in SM 8) involved in the transitions of the major peaks are shown in Fig. 16.

The vertical excitations with their band position, oscillator strength and character assignment from TDFT are presented in Table 3.

4. Conclusions

The anchoring ligand pcqH is relatively new. There are only a few examples [65] where this ligand has been used in a Ru based dye along with other popular anchoring groups, e.g. 2,2′-bipyridyl-4,4′-dicarboxylic acid, 2,2′2″-terpyridyl-4,4′,4″-tricarboxylic acid etc. As a single anchoring group this report may be the first one where the anchoring takes place through the 2-(2-pyridyl)-4-carboxyquinoline ligand (pcqH). The synthesis of this anchoring ligand is quite simple. The complete synthesis of the dye requires no complicated approach, like the use of cross-coupling chemistry, thus bringing down the cost of the preparation to a minimum. The purification is done on silica without any prior treatment, which is again unusual for the purification of ruthenium dyes where normally a Sephadex column is required.

The dye shows a very prominent red shifted MLCT (536 nm), $\varepsilon = 17 \times 10^3\ M^{-1}\ cm^{-1}$. This dye is a promising candidate for PV energy conversion in terms of IV, %FF and %IPCE character. It is envisaged that with suitable modification in the anchoring sites, better substitutions on the phenyl group attached to the central pyridine ring of the terpyridine ligand and coordination with different ancillary ligands, there is further scope of improvement of the efficiency of this dye.

Acknowledgements

SN acknowledges AICTE, New Delhi, India. This work was funded from the AICTE-RPS grant: 8023/RID/RPS-10/Pvt (II Policy)/2011-12. SN also acknowledges the NMR spectral facility and Computational Chemistry facility established in the Chemistry Dept. BIT-Mesra through the DST FIST Program (SR/FST/CSI-242/2012). Different analytical services obtained from CIF, BIT-Mesra is greatly acknowledged. JD acknowledges DST-SERI, New Delhi-110016. T.K.M. thanks CSIR for research funding through CSIR-EMR (Project Nos. 01(2470)/11/EMR-II.

Appendix A. Supplementary data

All the structural characterizations, namely mass, ^1H and ^{13}C NMR data, molecular orbital diagrams of the optimized structure and redox potential data. Supplementary data associated with this article can be found, in the online version, at http://dx.doi.org/10.1016/j.poly.2015.10.040.

References

[1] J. Barber, Q. Rev. Biophys. 36 (2003) 71.
[2] E. Baranoff, J.-P. Collin, L. Flamigni, J.-P. Sauvage, Chem. Soc. Rev. (2004) 147.
[3] T.A. Moore, D. Gust, P. Mathis, J.-C. Mialocq, C. Chachaty, R.V. Bensasson, E.J. Land, D. Doizi, P.A. Liddell, W.R. Lehman, G.A. Nemeth, A.L. Moore, Nature 307 (1984) 630.
[4] K. Kalyansundaram, Photochemistry of Polypyridine and Porphyrin Complexes, Academic Press Limited, 1991. Chapter 6.
[5] P.A. Anderson, F.R. Keene, T.J. Meyer, J.A. Moss, G.F. Strouse, J.A. Treadway, J. Chem. Soc., Dalton Trans. (2002) 3820.
[6] A. Hagfeldt, M. Gratzel, Acc. Chem. Res. 33 (2000) 269.
[7] K. Kalyanasundaram, M. Graetzel, M.K. Nazeeruddin, Inorg. Chem. 31 (1992) 5243.
[8] J.V. Caspar, T.J. Mayer, Inorg. Chem. 2 (1983) 2444.
[9] M. Hang, V. Huynh, D.M. Dattelbaum, T.J. Meyer, Coord. Chem. Rev. 249 (2005) 457.
[10] T.J. Meyer, Pure Appl. Chem. 58 (1988) 1193.
[11] L. Spiccia, G.B. Deacon, C.M. Kepert, Coord. Chem. Rev. 248 (2004) 1329.
[12] J.V. Caspar, T.J. Meyer, J. Am. Chem. Soc. 105 (1983) 5583.
[13] K. Kalyanasundaram, M.K. Nazeeruddin, Inorg. Chem. 29 (1990) 1888.
[14] A.M.W. Cargill Thompson, M.C.C. Smailes, J.C. Jeffery, M.D. Ward, J. Chem. Soc., Dalton Trans. (1997) 737.
[15] V. Aranyos, J. Hjelm, A. Hagfeldt, H. Grennberg, J. Chem. Soc., Dalton Trans. (2003) 1280.
[16] O.S. Odongo, M.M. Allard, H.B. Schlegel, J.F. Endicott, Inorg. Chem. 49 (2010) 9095.
[17] E.C. Constable, R.W. Handel, C.E. Housecroft, A.M. Morales, L. Flamigni, F. Barigelletti, J. Chem. Soc., Dalton Trans. (2003) 1220.
[18] C.J. Elsevier, J. Reedijk, P.H. Walton, M.D. Ward, Dalton Trans. (2003) 1869.

[19] A. Juris, V. Balzani, F. Barigelletti, S. Campagna, P. Belser, A. Von Zelewsky, Coord. Chem. Rev. 84 (1988) 85.
[20] J.-P. Sauvage, J.-P. Collin, J.C. Chambron, S. Guillerez, C. Coudret, V. Balzani, F. Barigelletti, L. De Cola, L. Flamigni, Chem. Rev. 94 (1994) 993.
[21] J.R. Winkler, T.L. Netzel, C. Creutz, N. Sutin, J. Am. Chem. Soc. 109 (1987) 2381.
[22] D.P. Rillema, D.S. Jones, C. Woods, H.A. Levy, Inorg. Chem. 31 (1992) 2935.
[23] S. Pyo, E. Perez-Cordero, S.G. Bott, L. Echegoyen, Inorg. Chem. 38 (1999) 3337.
[24] J.M. Calvert, J.V. Caspar, R.A. Binstead, T.D. Westmoreland, T.J. Meyer, J. Am. Chem. Soc. 104 (1982) 6620.
[25] M. Maestri, N. Armaroli, V. Balzani, E.C. Constable, A.M.W. Cargill Thompson, Inorg. Chem. 34 (1995) 2759.
[26] P. Laine, F. Bedioui, E. Amouyal, V. Albin, F. Berruyer-Penaud, Chem. Eur. J. 8 (2002) 3162.
[27] Y.-Q. Fang, N.J. Taylor, G.S. Hanan, F. Loiseau, R. Passalacqua, S. Campagna, H. Nierengarten, A. Van Dorsselaer, J. Am. Chem. Soc. 124 (2002) 7912.
[28] E.A. Medlycott, G.S. Hanan, Chem. Soc. Rev. 34 (2005) 133.
[29] C.R. Hecker, A.K.I. Gushurst, D.R. McMillin, Inorg. Chem. 30 (1991) 538.
[30] G.F. Strouse, J.R. Schoonover, R. Duesing, S. Boyde, W.E. Jones Jr., T.J. Meyer, Inorg. Chem. 34 (1995) 473.
[31] S.H. Wadman, J.M. Kroon, K. Bakker, M. Lutz, A.L. Spek, G.P. van Klink, G. van Koten, Chem. Commun. (2007) 1907.
[32] S.H. Wadman, J.M. Kroon, K. Bakker, R.W.A. Havenith, G.P.M. van Klink, G. van Koten, Organometallics 29 (2010) 1569.
[33] K.C.D. Robson, B.D. Koivisto, A. Yella, B. Sporinova, M.K. Nazeeruddin, T. Baumgartner, M. Grätzel, C.P. Berlinguette, Inorg. Chem. 50 (2011) 5494.
[34] M.K. Nazeeruddin, E. Müller, R. Humphry-Baker, N. Vlachopoulos, M. Grätzel, J. Chem. Soc., Dalton Trans. (1997) 4571.
[35] M.K. Nazeeruddin, A. Kay, L. Rodicio, R. Humpbry-Baker, E. Miiller, P. Liska, N. Vlachopoulos, M. Gratzel, J. Am. Chem. Soc. 115 (1993) 6382.
[36] E. Jakubikova, W. Chen, D.M. Dattelbaum, F.N. Rein, R.C. Rocha, R.L. Martin, E.R. Batista, Inorg. Chem. 48 (2009) 10720.
[37] G.C. Vougioukalakis, A.I. Philippopoulos, T. Stergiopoulos, P. Falaras, Coord. Chem. Rev. 255 (2011) 2602 (and all the references therein).
[38] T.W. Rees, E. Baranoff, Polyhedron 82 (2014) 37.
[39] V. Shklover, M.K. Nazeeruddin, M. Gratzel, Y.E. Ovchinnikov, Appl. Organomet. Chem. 16 (2002) 635.
[40] D.J. Wasylenko, C. Ganesamoorthy, B.D. Koivisto, M.A. Henderson, C.P. Berlinguette, Inorg. Chem. 49 (2010) 2202.
[41] B.S. Furniss, A.J. Hannaford, P.W.G. Smith, A.R. Tatchell, Vogels Textbook of Practical Organic Chemistry, 5th ed., ELBS with Longman, 1989. 399.
[42] D.T. Sawyer, A. Sobkowiak, J.L. Roberts Jr., Electrochemistry for Chemists, 2nd ed., John Wiley & Sons, New York, 1995. 333.
[43] J. Wang, G.S. Hanan, Synlett (2005) 1251.
[44] A.A. Farah, J.G.C. Veinot, M. Najman, W.J. Pietro, J. Macromol. Sci., Pure Appl. Chem. 11 (A37) (2000) 1507.
[45] S. Ito, P. Chen, P. Comte, M.K. Nazeeruddin, P. Liska, P. Pechy, M. Gratzel, Prog. Photovoltaics 15 (2007) 603.
[46] F. Santiagoa, J. Bisquerta, G. Garcia-Belmonte, G. Boschloo, A. Hagfeldt, Sol. Energy Mater. Sol. Cells 87 (2005) 117.
[47] K.D. Seo, I.T. Choi, Y.G. Park, S. Kang, J.Y. Lee, H.K. Kim, Dyes Pigm. 94 (2012) 469.
[48] J.-Y. Kim, J.Y. Kim, D.-K. Lee, B. Kim, H. Kim, M.J. Ko, J. Phys. Chem. C 43 (116) (2012) 22759.
[49] M.J. Frisch, G.W. Trucks, H.B. Schlegel, G.E. Scuseria, M.A. Robb, J.R. Cheeseman, J.A. Montgomery, T. Vreven Jr., K.N. Kudin, J.C. Burant, J.M. Millam, S.S. Iyengar, J. Tomasi, V. Barone, B. Mennucci, M. Cossi, G. Scalmani, N. Rega, G.A. Petersson, H. Nakatsuji, M. Hada, M. Ehara, K. Toyota, R. Fukuda, J. Hasegawa, M. Ishida, T. Nakajima, Y. Honda, O. Kitao, H. Nakai, M. Klene, X. Li, J.E. Knox, H. P. Hratchian, J.B. Cross, C. Adamo, J. Jaramillo, R. Gomperts, R.E. Stratmann, O. Yazyev, A.J. Austin, R. Cammi, C. Pomelli, J.W. Ochterski, P.Y. Ayala, K. Morokuma, G.A. Voth, P. Salvador, J.J. Dannenberg, V.G. Zakrzewski, S. Dapprich, A.D. Daniels, M.C. Strain, O. Farkas, D.K. Malick, A.D. Rabuck, K. Raghavachari, J.B. Foresman, J.V. Ortiz, Q. Cui, A.G. Baboul, S. Clifford, J. Cioslowski, B.B. Stefanov, G. Liu, A. Liashenko, P. Piskorz, I. Komaromi, R.L. Martin, D.J. Fox, T. Keith, M.A. Al-Laham, C.Y. Peng, A. Nanayakkara, M. Challacombe, P.M.W. Gill, B. Johnson, W. Chen, M.W. Wong, C. Gonzalez, J.A. Pople, Gaussian 09, Gaussian Inc., Wallingford, CT, 2004.
[50] N.M. O'Boyle, A.L. Tenderholt, K.M. Langner, J. Comp. Chem. 29 (2008) 839.
[51] T. Le Bahers, E. Brémond, I. Ciofini, C. Adamo, Phys. Chem. Chem. Phys. 16 (2014) 14435.
[52] M.K. Nazeeruddin, F. De Angelis, S. Fantacci, A.S. Guido Viscardi, P. Liska, S. Ito, B. Takeru, M. Gratzel, J. Am. Chem. Soc. 127 (2005) 16835.
[53] P.J. Giordano, C.R. Bock, M.S. Wrighton, J. Am. Chem. Soc. 100 (1978) 6960.
[54] K.J. Takeuchi, M.S. Thomson, D.W. Pipes, T.J. Meyer, Inorg. Chem. 23 (1984) 1845.
[55] A. Llobet, P. Doppelt, T.J. Meyer, Inorg. Chem. 27 (1988) 514.
[56] W.M. Clark, Oxidation-Reduction Potentials of Organic Systems, Williams & Wilkins, Baltimore, MD, 1960 (Ch. 4).
[57] X. Xiaoming, M. Haga, T. Matsumura-Inoue, Y. Ru, A.W. Addison, K. Kano, J. Chem. Soc., Dalton Trans. (1993) 2477.
[58] V. Shklover, M.K. Nazeeruddin, M. Gratzel, Y.E. Ovchinnikov, Appl. Organomet. Chem 16 (2002) 635.
[59] T. Bessho, E. Yoneda, J. Yum, M. Guglielmi, I. Tavernelli, H. Imai, U. Rothlisberger, M.K. Nazeeruddin, M. Grätzel, J. Am. Chem. Soc. 16 (131) (2009) 5930.
[60] D.V. Pogozhev, M.J. Bezdek, P.A. Schauer, C.P. Berlinguette, Inorg. Chem. 6 (52) (2013) 3001.
[61] K.L. Wu, H.C. Hsu, K. Chen, Y. Chi, M. Chung, W. Liub, P. Chou, Chem. Commun. 46 (2010) 5124.
[62] M.W. Cooke, G.S. Hanan, F. Loiseau, S. Campagna, M. Watanabe, Y. Tanaka, J. Am. Chem. Soc. 129 (2007) 10479.
[63] E. Jakubikova, W. Chen, D.M. Dattelbaum, F.N. Rein, R.C. Rocha, R.L. Martin, E.R. Batista, Inorg. Chem 48 (2009) 10720.
[64] A.A. Farah, W.J. Pietro, Inorg. Chem. Commun. 6 (2003) 662.
[65] S. Altobello, R. Argazzi, S. Caramori, C. Contado, S. Da Fre', P. Rubino, C. Choné, G. Larramona, C.A. Bignozzi, J. Am. Chem. Soc. 127 (2005) 15342.